Dynamics of the Phase Inversion Process

A. J. McHUGH* and C. S. TSAY†

Department of Chemical Engineering, University of Illinois, Urbana, Illinois 61801

SYNOPSIS

An analysis of the dynamics of phase inversion based on mathematical modeling and *in situ* experimental observations is presented. Calculations based on ternary diffusion models illustrate the effects of casting film composition, evaporation time, and film thickness on the precipitation time and resulting polymer film profiles, which correlate with observed final morphologies. An experimental method based on the use of dark ground optics, interface visualization, and reflected light illumination is used for *in situ* monitoring of the mass transfer and phase separation dynamics during the quench step. Observations on the systems water–dimethylsulfoxide–cellulose acetate and water–dioxane–cellulose acetate show regions in the films corresponding to gel formation and growth, instabilities associated with finger formation, and homogeneous ternary diffusion. Data for the kinetics of the diffusion and gel front motions show that both propagate as the square root of time with rates dependent on the bath–film compositions. Examples of interface structures characteristic of deep quenching and nucleated droplet growth are also shown. Semiquantitative analyses in terms of the ternary models developed earlier and a phenomenological model for diffusion in the growing gel are used to explain the trends seen. © 1992 John Wiley & Sons, Inc.

INTRODUCTION

Quantitative analysis of the evaporation and quench periods is essential for understanding the morphology development that takes place during phase inversion. Such knowledge has direct application in the processing of asymmetric membranes, however, the scientific and technological base extends to a number of other important polymer processes such as wet spinning, gel spinning, and so-called phase separation spinning.[1]

In the last few years, significant progress has been made in the mathematical modeling of phase inversion through application of ternary diffusion theory to the quench step,[2-4] and, more recently, the combined evaporation and quench steps.[5] As a result, we now have the ability to calculate the dynamics of the process prior to phase separation in terms of measurable transport and thermodynamic parameters. Quantities such as composition paths, precip-

itation times, and associated concentration profiles in the polymer film can be correlated directly with morphologies that have been observed under a wide range of processing conditions.[4] Observations concerning phase separation phenomena in the structuring, as well as the role of spinodal decomposition and nucleation and growth mechanisms can now be put on a more firm, quantitative basis for comparison to processing conditions.[6]

On the other hand, since most experimental studies have been confined to observations of formed morphologies, inferences concerning the dynamics of the structure formation have been largely qualitative. With the exception of a few early observations,[7] *in situ* measurements of the mass transfer and phase separation have been lacking. In our laboratory, we have developed methods based on dark ground optics, reflected light illumination, and interface visualization, in combination with video image processing, to monitor the mass transfer and phase separation processes that take place in polymer films during the quench period. The purpose of this work is to present significant new results from our film quenching studies along with a discussion of their implications for understanding and modeling

the dynamics of the phase inversion process. A companion article reports observations of the bath-side transfer processes.[8] We begin with a brief review of some pertinent modeling results.

COMPREHENSIVE MODEL FOR PHASE INVERSION

A schematic of the one-dimensional geometry used for modeling the casting system is shown in Figure 1. For the evaporation step the surrounding medium is air, and, for the quench step, it is the coagulation bath. The model assumes constant partial specific volume, Fickian diffusion, equilibrium at the air–film or bath–film interface, and ideal gas behavior in the vapor phase. The ternary thermodynamics is based on modified Flory–Huggins theory with concentration-dependent interaction parameters. Complete descriptions of the binary diffusion equation formalism used in the evaporation step[9] and the combined film-side, ternary, and bath-side binary diffusion equations for the quench period,[5] along with discussions of the associated parameters, are given in the noted references.

Generally speaking, parameters related to the initial film dimensions, vapor concentration, and mass transfer in the casting atmosphere are important for the evaporation period, while those associated with the initial film and bath compositions are of importance in the quench period. For a given set of conditions, one is interested in the time at which a concentration path on the phase diagram first crosses the liquid miscibility gap (instantaneous vs. delayed precipitation) and the associated polymer profile in the film at the precipitation time. Key predictions from these profiles include film shrinkage (related to the film thickness), skin surface density (related to the polymer interface concentration), skin thickness (the appropriate thickness
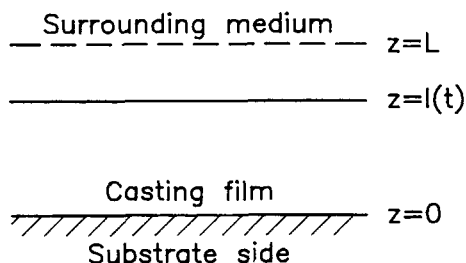
Surrounding medium   z=L

z=l(t)

Casting film
z=0

Substrate side

Figure 1 Schematic of phase inversion model geometry. Initial film interface is at L; $l(t)$ is the medium–film interface position at time t.
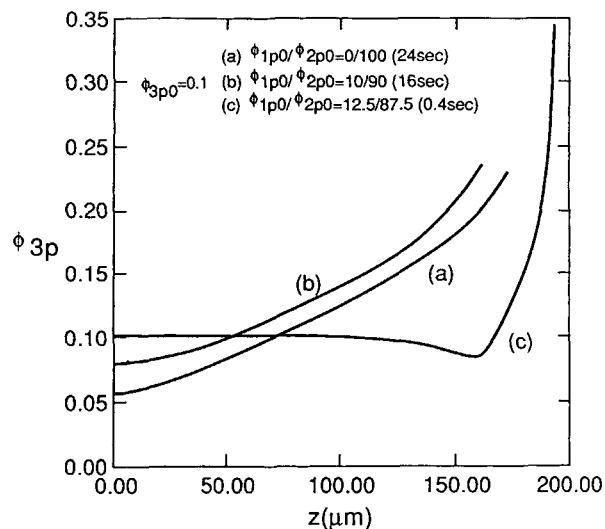
Figure 2 Calculated cellulose acetate volume fraction profiles (component 3) in polymer films at the point of precipitation (precipitation time noted in parentheses) for various nonsolvent(1)(water)–solvent(2)(acetone) initial compositions in quenched films. Profiles (a) and (b) correspond to delayed precipitation; profile (c) is rapid precipitation. In each case the initial cast film thickness is 200 μm.

of the high polymer concentration region near the interface), and sublayer structure (the polymer bulk concentration profile).

Water–acetone–cellulose acetate is a membrane-forming system for which all model parameters associated with the evaporation and quench steps can be evaluated from literature data. Details are given in our earlier studies.[4,5,9] Since diffusion coefficients can vary by more than two orders of magnitude throughout the diffusion domain, accounting for composition dependence is important. The four ternary diffusion coefficients are evaluated through the composition dependencies of the three interaction parameters, g_{ij}, and the three independent friction coefficients, ζ_{ij}'s, as well as free volume parameters associated with the self-diffusion coefficients based on limiting binary pairs. Two examples of interest for illustration are the effect of the nonsolvent–solvent ratio in the cast film in the absence of evaporation and the effect of cast film thickness in the presence of an evaporation period.

Figure 2 shows that the addition of nonsolvent to the casting solution eventually induces a transition in the dynamics from delayed to rapid precipitation. The uniformity of the profiles corresponding to delayed precipitation [i.e., (a) and (b)], should result in phase separation throughout the bulk of the film leading to similar sponge-type morphologies.

The increase in initial nonsolvent concentration under these conditions also leads to increased film shrinkage due to decreases in the nonsolvent inflow rate. Profile (c), on the other hand, corresponds to rapid precipitation and indicates the likelihood of fingering instability. As a result of the steep gradient near the interface, formation of a very thin skin would be expected. Such a skin would be susceptible to rupture leading to rapid growth of nonsolvent "fingers" in the relatively low viscosity (low polymer concentration) bulk beneath. The predictions of these calculations correspond with scanning electron microscopy (SEM) observations reported by Reuvers[10] for the same system, thus demonstrating the utility of the model as a means for correlating membrane structure formation with casting conditions.

Calculations[5] show that property changes with film thickness will be significant in the presence of an evaporation step. Figure 3 shows an example that illustrates that, for a constant evaporation time (20 s), decreases in the casting film thickness lead to an increase in the skin density, sublayer asymmetric porous structure, and film shrinkage, and a simultaneous decrease in the skin thickness. Each of these profiles corresponds to precipitation times in excess of 10 s (i.e., delayed precipitation). High interface concentration, steep gradients near the interface, and more importantly, high polymer concentrations underneath the skin area, should lead to a corresponding increase in resistance to the instabilities leading to finger structure formation.[11] Thus through

Figure 4 Diffusion cell consisting of aluminum chamber (B), optical glass chamber (C), frame (A), pressure block (H), and separating plate (F). Cavity (E) is filled with denser solution and block (G) aligns chamber cavities (D) and (E) prior to removal of the separating plate.

a combination of decreased initial film thickness and an appropriate evaporation step, both selectivity and permeability of the resulting membrane can be improved. One also finds that final membrane structure is quite sensitive to the evaporation time with significant membrane property changes expected as a result of a 20-s evaporation period.

EXPERIMENTAL

Materials

Polymer solutions were prepared using cellulose acetate (CA-398-3, Eastman Kodak) having an average molecular weight, $\bar{M}_n = 30,000$ and an average acetyl content of 39.8%. Reagent-grade dimethyl sulfoxide and dioxane (Fisher Scientific) were used as solvents. The nonsolvent was deionized, distilled water.

Diffusion Cell

The relevant quantities one wishes to monitor in the polymer film during the quench period include: diffusion front motion, film–bath interface motion, precipitation time, gelation front motion, and structure formation in the two-phase region. Complications in the diffusion cell design arise from the large initial viscosity differences and concentration gradients in the contacting phases along with potentially rapid phase separation. Figure 4 shows a sche-
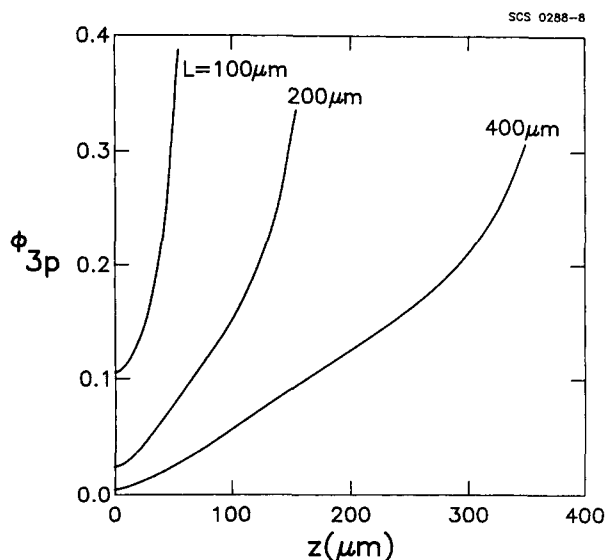
Figure 3 Effect of casting film thickness on cellulose acetate volume fraction profile at precipitation time for water quench preceded by 20 s evaporation period.
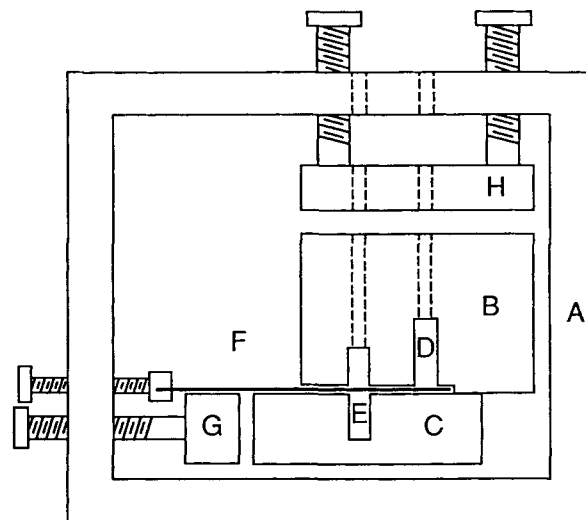
matic of the modified Lamm optical diffusion cell[12] that is used. The upper chamber (B) is made of aluminum and the lower chamber (C), in which diffusion is monitored, is made of optical quality fused silica (Hellma Cells Inc.). Both chambers are held together by the aluminum frame (A) and Teflon pressure block (H). The separating plate (F) is a 0.002-in.-thick, metal foil that is lubricated around the perimeter with a thin layer of vacuum grease to ensure leakage-proof operation. The lower cavity (E) is filled with denser solution and the upper cavity (D) is aligned using the pressure block (G) and filled with the less dense solution. Interfacial contact is achieved by removal of the separating plate using a motor-driven device.

In the case of membrane formation, additional experimental difficulties are related to the speed of the exchange process and the size scales of the regions one would like to probe. Fortunately, problems associated with the size and time scales are alleviated by an important characteristic of the diffusion process as indicated in our model equations,[4] namely, that all measurable quantities scale with the initial film thickness, L. In particular, precipitation time and mass transfer rate are proportional to L^2 and $1/L$, respectively. In addition, skin thickness and pore dimensions increase with increasing film thickness and film concentration profiles scale directly with L. Thus, the transport dynamics and related morphology development can be monitored using millimeter thick films. By appropriate scaling, such data can be applied to describe the behavior in films on the order of microns.

Optics

Figure 5 shows a schematic of the optical system. The objective lens, pinhole aperture, and collimating lens produce an expanded, noiseless beam of uniform intensity. Changes in the solution refractive index, $n(Y, t)$, induce a retardance, δ, in the light passing through the cell given by[13]:

$$\delta(Y, t) = \frac{2\pi w[n(Y, t) - n_R]}{\lambda} \quad (1)$$

where Y is the position in the lower solution relative to the initial interface, w is the cell thickness (4 mm), λ is the wavelength of light (632.8 nm) and the reference refractive index, n_R, is that of the initially uniform composition in the lower solution. The diffraction image of the phase-modulated beam emerging from the cell is filtered on the back focal plane of the transform lens with a circular stop to
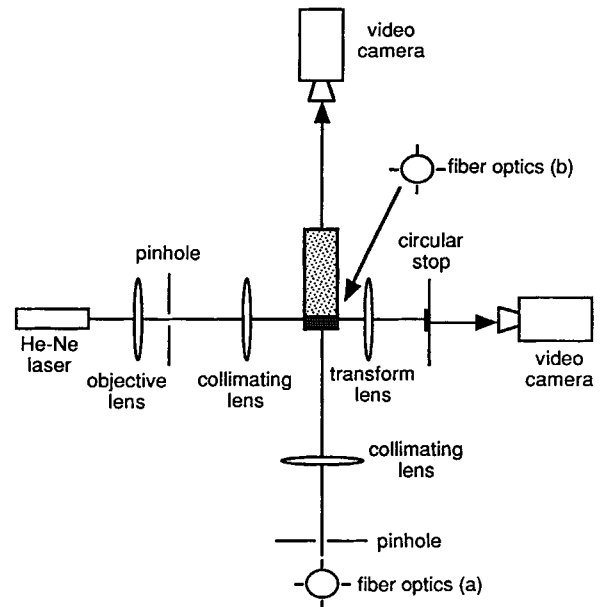

Figure 5 Schematic of optics for study of film transfer processes. The fiber optics (a) and (b) are used for interface visualization and reflected light illumination, respectively.

remove the unrefracted light image from the pinhole aperture. The stop is a 150-μm-diameter chromium disc that is evaporated onto a glass plate using a photolithographic technique.[14] The resultant filtered image is focused through the camera for recording of the fringe pattern superimposed on the cell. Proper adjustment of the stop position relative to the pinhole image is generally necessary in order to ensure that all of the refracted beam is included in the filtered diffraction pattern. Under such conditions, the relationship between the phase shift and fringe pattern intensity will be given by[15]

$$I(Y, t) = 4C^2 \sin^2\left[\frac{\delta(Y, t)}{2}\right] \quad (2)$$

where C is a constant associated with the optical elements.

From the dark ground image one can observe the refractive index distribution near the diffusion front and, depending on conditions, also distinguish finger formation from sponge formation. By simultaneously monitoring the reflected light image, the motion of the precipitation (gelation) front can also be followed. Finally, from image analysis of the transmitted light pattern, one can monitor precipitation time, the interface phase separation mechanism and membrane porosity. Morphological ob-

servations can be correlated with direct optical microscopy of the gel phase that is extracted from the diffusion cell at various points in the process.

Reproducibility and accuracy of the diffusion cell and optics have been established through measurement of binary diffusion coefficients following a technique described elsewhere.[16] In all cases agreement with literature results was good, assuring the reliability of the design.

RESULTS

Dark Ground Optics and Reflected Light Illumination

The combined dark ground and reflected light images give important qualitative and quantitative information on the diffusion and phase separation kinetics during the quench period. Figure 6 shows an example of a quench in which gelation, finger for-

mation, and homogeneous diffusion appear simultaneously. In this case the initial polymer solution was 10 vol % cellulose acetate (CA) in dimethyl sulfoxide (DMSO), and the contacting solution was pure water. Under these conditions, the precipitation is essentially instantaneous (i.e., rapid precipitation). The top, milky area is reflected light from a propagating opaque region that extends from the initial film–bath interface to the position Y_{gel}. Close examination of video images show the presence of vertical columns in the bulk of this region. These columns correspond to finger cavities seen in optical microscopy of the solid gel extracted from the cell at various points in the process. In addition, the overall thickness of the milky region corresponds exactly to that of the extracted solid. We thus associate the reflected light with the region of solid gel. The dark area directly beneath the gel front is a fluid single-phase or two-phase region in the film where gradients are sufficiently large to refract light beyond the camera lens aperture. The bright band
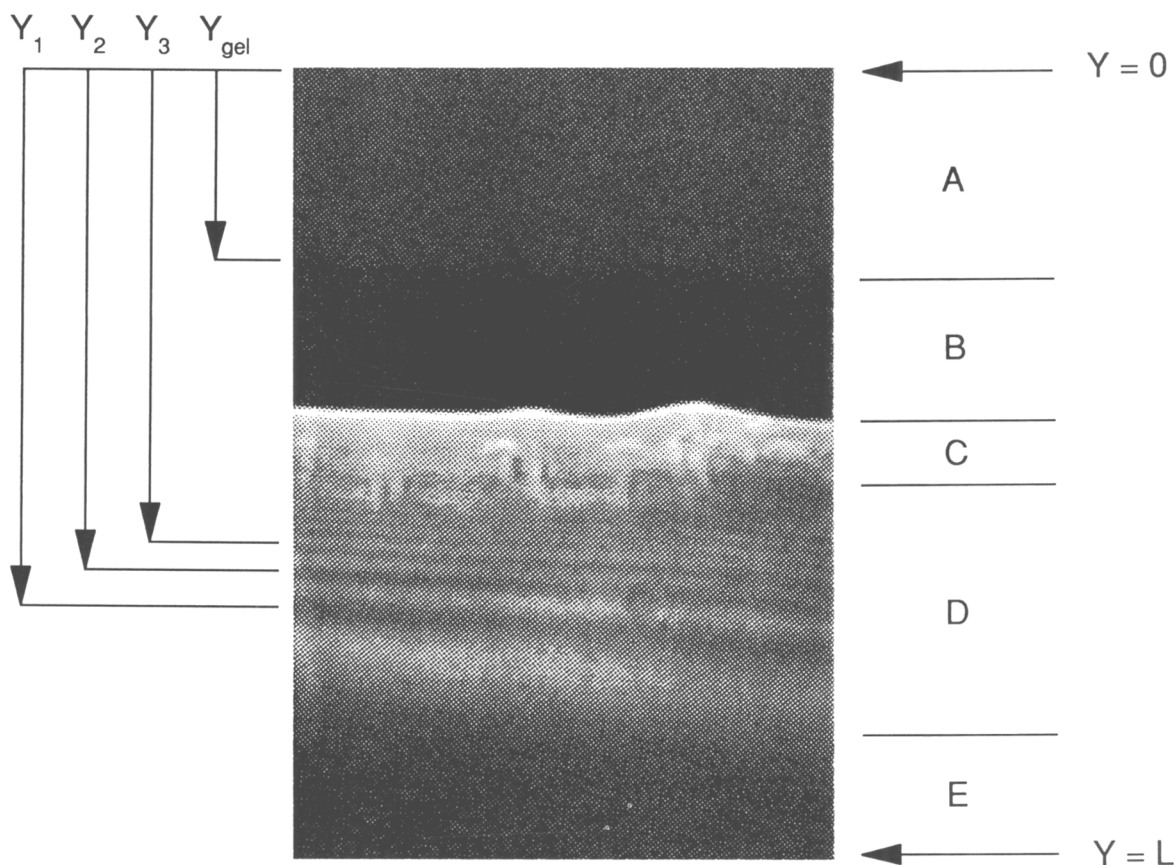

Figure 6 Combined dark ground and reflected light images of 10 vol % CA/DMSO film ($L = 3.02$ mm) quenched in pure water. Five regions are seen: (A) gel (milky region on top), (B) dark band (camera lens aperture limit), (C) bright band with striations, (D) homogeneous diffusion fringe pattern, and (E) dark region (corresponding to initial homogeneous solution).

immediately below this area indicates the beginning of the dark ground pattern. Regions of striations in the upper part of the pattern in this area correspond to finger cavities in the solid gel. The uniform fringe pattern beneath the striations is due to refractive index changes generated by the homogeneous ternary diffusion where Y_1, Y_2, and Y_3 represent the positions of the first-, second-, and third-order fringe intensity minima. Finally, the bottom, dark area represents the uniform concentration portion of the film into which the diffusion front has yet to propagate.

Quantitative data for the dynamics of the homogeneous diffusion and gel front motions of Figure 6 are shown in Figure 7. The top three data sets show that all three fringe minima propagate as the square root of time. Precise location of the minimum position within a given fringe was determined using video imaging methodology described elsewhere.[17] The accuracy of location of a minimum is ±0.01 mm with this method and the time accuracy is ±0.05 s. The gel front is also seen to move with a square root of time dependence up to about 60% of the film thickness, after which it accelerates due to the finite film thickness. Figures 8 and 9 show the effects of increasing the initial polymer concentration in the film and initial solvent concentration in the water bath, respectively. In both cases, the square root of time dependence is maintained, however, the slope decreases with increases in either polymer or solvent concentration. As seen in Figure
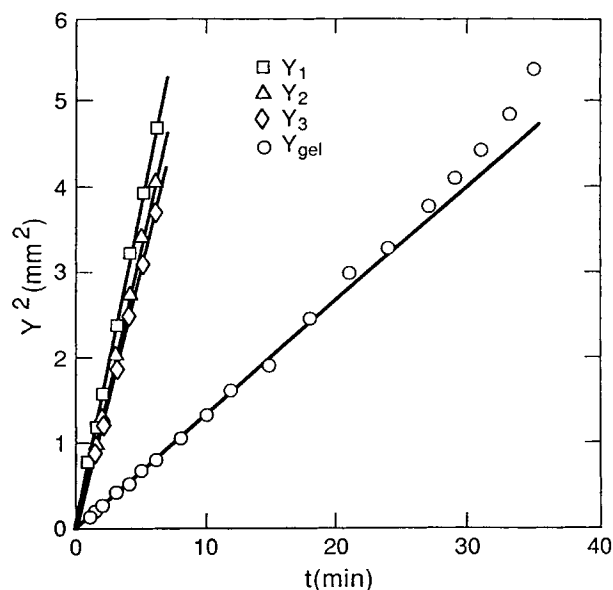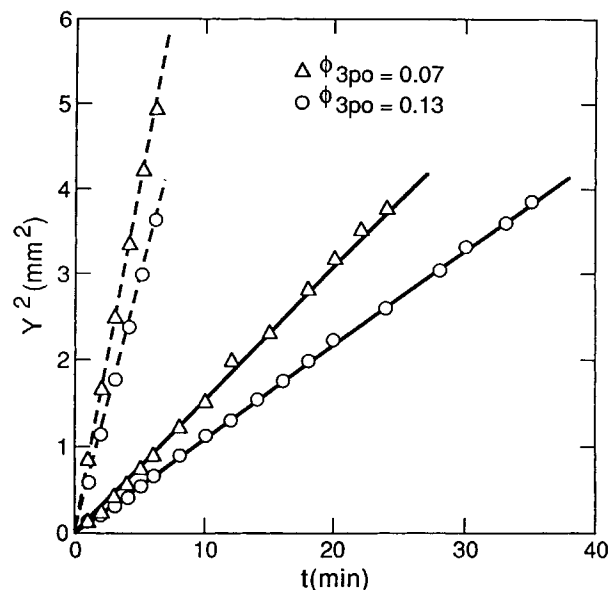

Figure 8 Time-dependent motions of first-order diffusion fringes (dashed lines) and gel front (solid lines) in CA/DMSO films as a function of initial polymer concentration for pure water quench.

10, the velocity of the gelation front also decreases as solvent changes from DMSO to dioxane (i.e., decreasing solubility gap in ternary phase diagram).

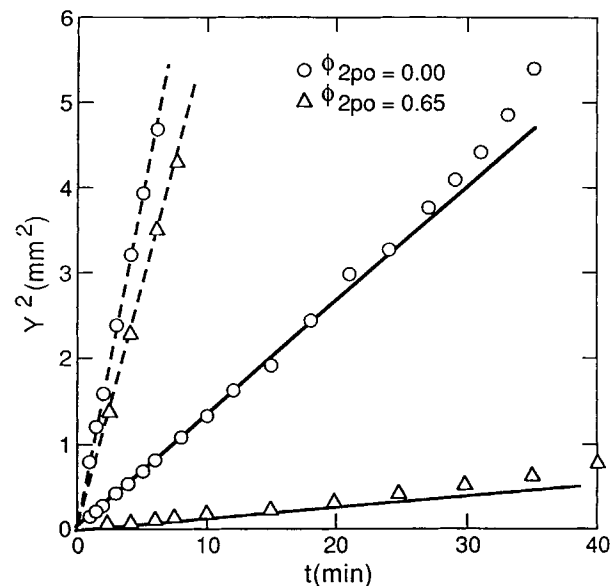Figure 11 shows the appearance of the film regions

Figure 7 Time-dependent motions of diffusion fringes and gel front under conditions of Figure 6.

Figure 9 Time-dependent motions of first-order diffusion fringes (dashed lines) and gel front (solid lines) as a function of initial solvent concentration in quench bath for 10 vol % CA/DMSO films.
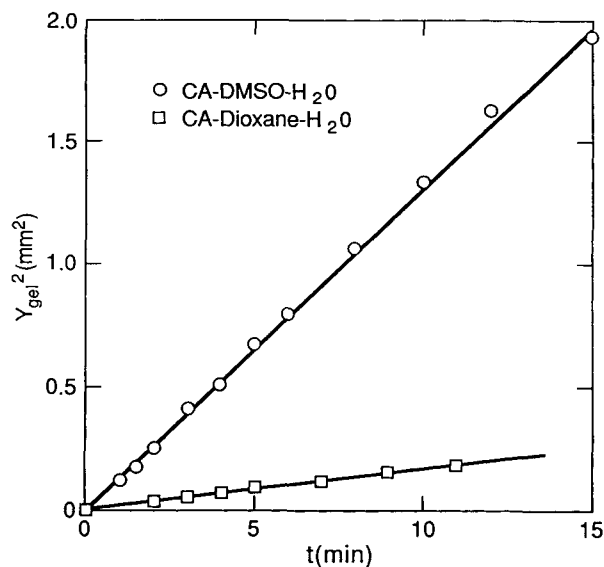
DYNAMICS OF THE PHASE INVERSION PROCESS   **2017**

Figure 10 Comparison of gel front motion for CA–DMSO–water and CA–dioxane–water systems. Initial polymer concentrations in both cases was 10 vol % in solvent quenched in pure water.

under quench conditions associated with finger formation (rapid precipitation) [Fig. (a)] and spongy structure formation (delayed precipitation) [Fig. (b)]. In the latter case the diffusion and gel front motions are seen to be more uniform. In addition, both the gel phase and dark ground interface regions show a lack of striations. Figure 11 also demonstrates that the delayed precipitation film undergoes greater shrinkage, a result that is in agreement with our model predictions (see Fig. 2).

Figure 12 illustrates the effect of initial film thickness on the motion of the gel front, Y_{gel}, as measured from the initial film–bath interface. In all three cases the front moves initially as the square root of time; however, with decreasing initial film thickness, the position of departure from the square root dependence moves to lower times. An important result is shown in Figure 13, which demonstrates that gel motion for different initial film thicknesses displays a universal behavior pattern when plotted against the appropriate nondimensionalizing parameters. D_c has units of a characteristic diffusivity; its magnitude is 1.67×10^{-5} cm^2/s for these data and those shown in the following figure. As shown in Figure 14, such superposition also occurs for different initial bath concentrations. These results demonstrate the validity of our postulate that diffusion-controlled phenomena can be universally quantified in terms of appropriate length and time scales. The data in these two figures are also of considerable practical importance since they provide a basis for predicting time constants associated with gelation in the quench bath for a wide variety of conditions.
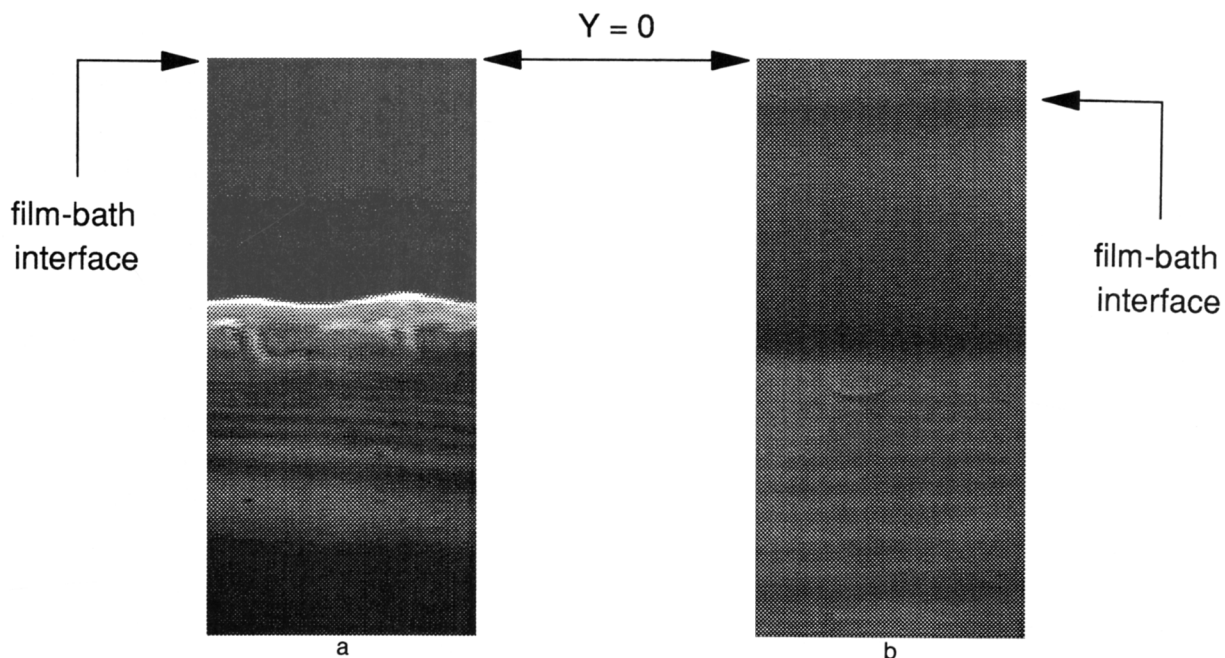

Figure 11 Appearance of (a) fast and (b) delayed precipitation films during phase inversion dynamics. (a) Pure water quench. (b) 76 vol % DMSO in bath.
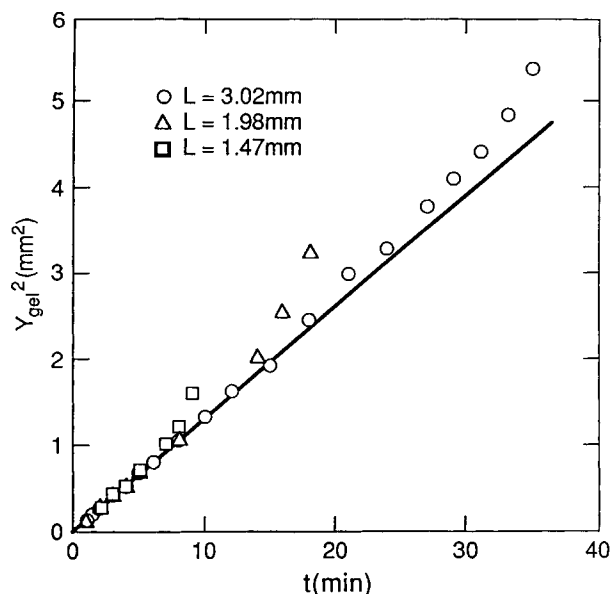
Figure 12 Effect of initial film thickness on gel front motion for 10 vol % CA–DMSO films quenched in pure water.

Interface Structure Formation

Interface visualization gives information on the precipitation time and associated phase separation mechanisms. Under conditions where the light transmittance remained finite for measurable times, plots of image intensity (averaged over a portion of the film) versus time were used to delineate rapid and delayed precipitation.
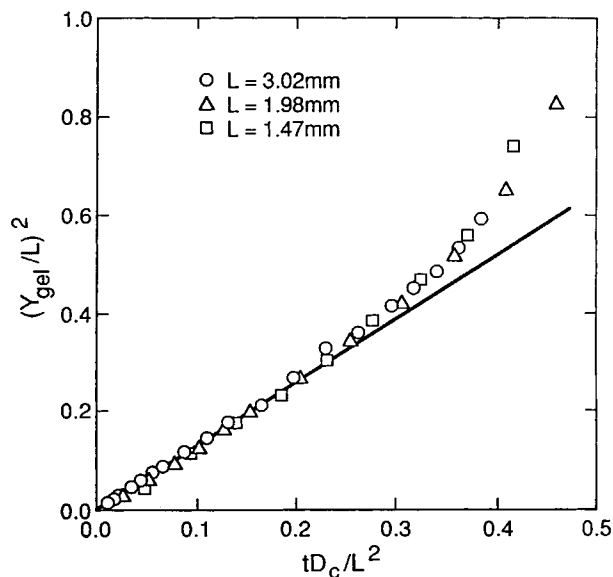

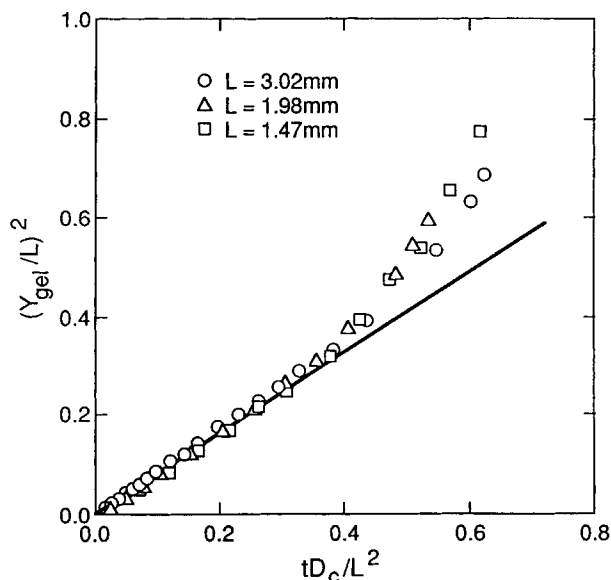**Figure 13** Dimensionless plot of data from Figure 12.

Figure 14 Dimensionless plot of gel front motion for 10 vol % CA solutions quenched in 35 vol % DMSO–water solutions for various initial film thicknesses.

Figure 15 illustrates the phase-separated structure that forms at the interface for two different polymer concentrations. The morphology on the left shows the lacy structure characteristic of deep quenching[18] while that on the right shows the nucleated growth of spheres of the nonsolvent-rich phase. Representative measurements of the diameter of the spherical regions in the latter case, shown in Figure 16, indicate that over the observable size range ($d \geq 30$ μm) growth is essentially linear with time up to about a diameter of 100 μm, after which further growth ceases. The appearance of an asymptotic value correlates with gel solidification, a point that will be discussed further in the following section.

The behavior shown in the two photos of Figure 15 is consistent with our earlier mass transfer–thermodynamic diagram considerations.[4] Lowering initial polymer concentration moves the mass transfer paths closer to the critical point where spinodal-like structure formation would be expected. Increased polymer concentrations lead to reduced transport rates and tend to move the point of precipitation to the metastable region of the phase diagram where nucleation and growth mechanisms predominate. In the case of lower initial polymer concentration, the interconnected network, in general, favors greater skin surface porosity resulting in higher membrane permeability and lower selectivity. These observations are in line with our model calculations[4] as well as experimental results for this system.[19]
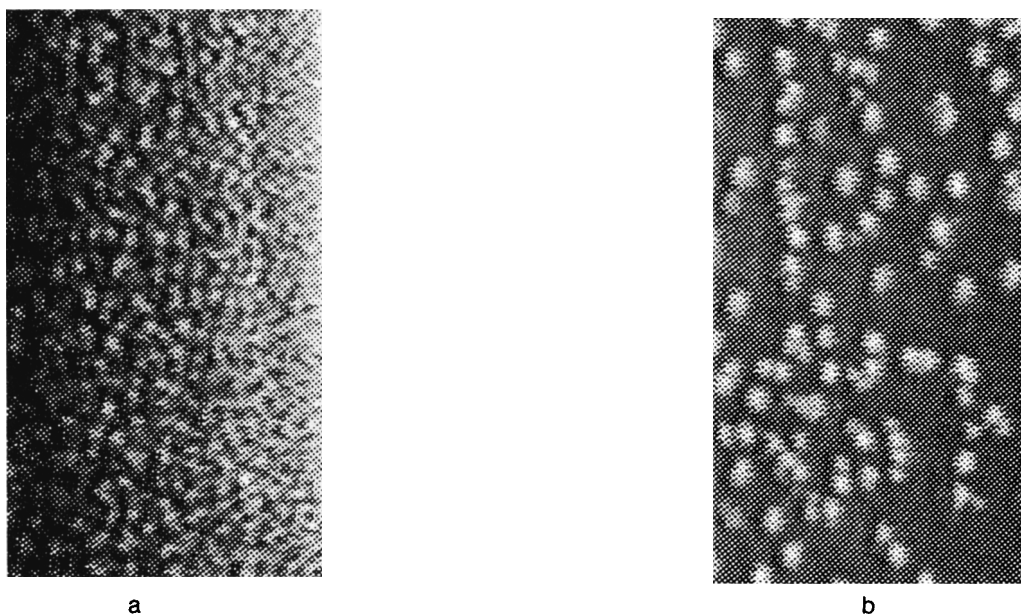
a   b

Figure 15   Effect of polymer concentration on interfacial structure formation. (a) 7 vol % CA, (b) 13 vol % CA.

DISCUSSION

The results presented in the previous sections represent, to our knowledge, the first complete experimental quantification of the diffusion and phase separation processes in a ternary phase inversion system. There are several aspects that merit discussion with respect to implications for the physics
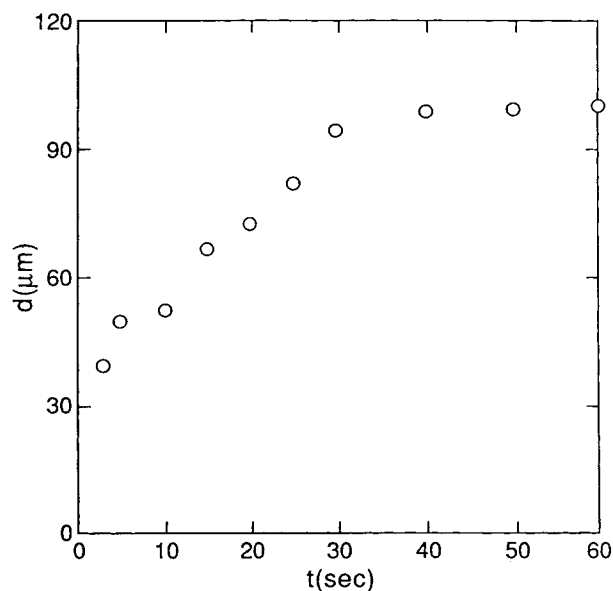

Figure 16   Measurements of the diameter of the spherical regions of Figure 15(b) as a function of time.

and modeling of the phase inversion process. For clarification, we refer to Figure 6 showing the measured diffusion and gel front motions (e.g., Y_1, Y_2, Y_3, and Y_{gel}), which will be discussed further.

The data in Figures 7–10 and 12–14 demonstrate that both the mass transfer and gelation processes in the film are diffusion controlled. The square root of time dependence for the diffusion front motion is a general result for homogeneous, one-dimensional diffusion in an infinite film, i.e., one in which the front has yet to propagate to the casting surface.[20] The dependence of the dimensionless composition profile on the Boltzmann transformation variable, $\zeta = Y/t^{0.5}$, also arises naturally from the ternary homogeneous diffusion equations discussed earlier as well as in the algorithm we have used to generate the initial front motion.[4] The trends shown in Figures 7, 8, and 9 are qualitatively consistent with the predictions of our model equations.

The motion of the gel front can similarly be rationalized by assuming that, for a given set of conditions, transport through the gelled region can be characterized in terms of a constant, Fickian diffusion coefficient that undergoes a discontinuity at a characteristic concentration, ϕ_{3pc}, separating the solidified gel from the ungelled, fluid region (see Figure 6). In addition, one needs to assume that the concentration at the gel–bath interface remains constant during the initial growth period, i.e., $\phi_{3p} = \phi_{3pt}$ at $Y = 0$. The resulting solutions to the diffusion problem and Y_{gel} are then given as[20]

$$\frac{\phi_{3pt} - \phi_{3pc}}{\phi_{3pc} - \phi_{3p0}} = \frac{G\left(\dfrac{K}{2\sqrt{\bar{D}_{gel}}}\right)}{F\left(\dfrac{K}{2\sqrt{\bar{D}_{fld}}}\right)} = \Phi\left(\frac{K}{\sqrt{\bar{D}_{fld}}}, \frac{\bar{D}_{fld}}{\bar{D}_{gel}}\right) \quad (3)$$

$$Y_{gel}(t) = K\sqrt{t} \quad (4)$$

where ϕ_{3p0} is the initial polymer composition in the film and K is a constant. G and F are functions of the dimensionless group consisting of K and the phenomenological diffusivities for the gel, $\bar{D}_{gel}$, and fluid, $\bar{D}_{fld}$, regions. These functions satisfy the following relationships:

$$G\left(\frac{K}{2\sqrt{\bar{D}_{gel}}}\right)$$
$$= \sqrt{\pi}\, \frac{K}{2\sqrt{\bar{D}_{gel}}} \exp\left(\frac{K^2}{4\bar{D}_{gel}}\right) \text{erf}\left(\frac{K}{2\sqrt{\bar{D}_{gel}}}\right) \quad (5)$$

and

$$F\left(\frac{K}{2\sqrt{\bar{D}_{fld}}}\right)$$
$$= \sqrt{\pi}\, \frac{K}{2\sqrt{\bar{D}_{fld}}} \exp\left(\frac{K^2}{4\bar{D}_{fld}}\right) \text{erfc}\left(\frac{K}{2\sqrt{\bar{D}_{fld}}}\right) \quad (6)$$

where erf and erfc are the error function and complementary error function. In these expressions, ϕ_{3p} refers now to total polymer composition at positions in the polymer film given by the additional subscripts. For constant $\bar{D}_{fld}/\bar{D}_{gel}$, Φ is a monotonically increasing function of $K/\bar{D}_{fld}^{0.5}$.

As such this model offers a phenomenological rationale for the initial square root of time dependence of the gel front motion as well as the fact that Y_{gel} scales as L, and times scale as L^2/D_c (Figs. 13 and 14). Two important assumptions are that for a given set of quench conditions the gel front is characterized by a fixed composition, ϕ_{3pc}, and the polymer composition at the film–bath interface remains constant during the square root of time growth period at a value $\phi_{3pt} > \phi_{3pc}$. With this in mind the principal effects of the casting variables can be interpreted through comparison to the model parameters. For example, Figures 8 and 9 show that the slope of the time dependence (i.e., K^2 in the phenomenological model) decreases with increases in either the initial polymer concentration in the film or the initial solvent concentration in the bath. In the latter case, one would expect $\bar{D}_{fld}$ and $\bar{D}_{gel}$ to remain relatively constant since the initial film composition remains

fixed. However, since addition of solvent to the bath will decrease the solvent flux from the film, the polymer composition at the interface, ϕ_{3pt}, must decrease. Therefore, under these conditions, Eq. (3) predicts that Φ must decrease, and in consequence a lower K value will result. In the case of increasing the initial polymer composition in the film, one would expect the composition variables on the left side of Eq. (3) to be affected more or less equally, hence Φ should remain fairly constant. On the other hand, the phenomenological coefficients, $\bar{D}_{fld}$ and $\bar{D}_{gel}$ should decrease since these now characterize diffusion through a more concentrated system. Hence, to maintain constancy of Φ, K must decrease.

Finally, the data in Figure 10 indicate that for smaller miscibility gap, i.e., the CA–dioxane–water system, a given mass transfer path will have to move further from the polymer–solvent axis before entering the gel region, thus decreasing the overall dimensionless composition ratio of Eq. (3), hence Φ. As a result the K value must decrease.

The primary emphasis in this work has been on semiquantitative explanations of the phenomena we have observed thus far in our studies of phase inversion in polymer films. Future studies will focus on direct quantitative comparisons to the predictions of our ternary diffusion model. Beyond correlating observed phenomena with given casting conditions, accurate analysis of the dynamics of phase inversion will enable more precise prediction of the processing parameters that control the development of a given polymer morphology having desirable end-use properties.

NOMENCLATURE

C Constant defined in Eq. (2)

d Diameter of the nucleated droplet (cm)

D_c Reference diffusivity for nondimensionalization (cm^2/s)

$\bar{D}_{fld}$ Phenomenological diffusivity for the fluid region (cm^2/s)

$\bar{D}_{gel}$ Phenomenological diffusivity for the gel region (cm^2/s)

F Function defined in Eq. (6)

g_{ij} Thermodynamic interaction parameter between components i and j

G Function defined in Eq. (5)

I Light intensity

K Slope of the Y_{gel} vs. $t^{0.5}$ curve $(cm/s^{0.5})$

l Time-dependent air–film or bath–film interface position (cm)

L Initial film casting thickness (cm)

$\bar{M}_n$ Number-average molecular weight

n Refractive index

t Time (s)

w Diffusion cell thickness (cm)

Y Position coordinate on film side relative to bath–film interface

z Vertical position coordinate relative to casting surface (cm)

δ Phase shift defined by Eq. (1)

ζ_{ij} Friction coefficient describing the interaction between components i and j $(g\ cm^3/s)$

λ Wavelength of light (cm)

ξ Boltzmann transformation variable $(cm/s^{0.5})$

ϕ_i Volume fraction of component i in liquid mixture

Φ Function defined in Eq. (3)

Subscripts

0   Initial value

1   Nonsolvent

2   Solvent

3   Polymer

c   Critical concentration for gelation

fld   Fluid region

gel   Gel region

p   Casting film side

R   Reference

t   Film–bath interface

REFERENCES

1. A. Ziabicki, *Fundamentals of Fibre Formation*, Wiley, New York, 1976.

2. L. Yilmaz and A. J. McHugh, *J. Memb. Sci.*, **28**, 287 (1986).

3. A. J. Reuvers, J. W. A. van den Berg, and C. A. Smolders, *J. Memb. Sci.*, **34**, 45 (1987).

4. C. S. Tsay and A. J. McHugh, *J. Polym. Sci. Polym. Phys. Ed.*, **28**, 1327 (1990).

5. C. S. Tsay and A. J. McHugh, *J. Polym. Sci. Polym. Phys. Ed.*, **29**, 1261 (1991).

6. C. S. Tsay and A. J. McHugh, *J. Polym. Sci. Polym. Phys. Ed.*, **30**, 309 (1992).

7. M. E. Epstein and A. J. Rosenthal, *Text. Res. J.*, **36**, 813 (1966); M. E. Frommer and D. A. Lancet, in *Reverse Osmosis Membrane Research*, H. K. Lonsdale and H. E. Podall, Eds., Plenum, New York, 1972, p. 85; H. Strathmann, K. Kock, and P. Amar, *Desalination*, **16**, 179 (1975).

8. G. E. Gaides and A. J. McHugh, *J. Memb. Sci.*, to appear.

9. C. S. Tsay and A. J. McHugh, *J. Memb. Sci.*, **64**, 181 (1991).

10. A. J. Reuvers, Ph.D. Dissertation, Twente University of Technology, Enschede, The Netherlands (1987).

11. H. Strathmann, in *Membranes and Membrane Processes*, E. Drioli and M. Nakagaki, Eds., Plenum Press, New York, 1986, p. 115.

12. H. J. V. Tyrrell and K. R. Harris, *Diffusion in Liquids*, Butterworths, London, 1984.

13. M. V. Klein and T. E. Furtak, *Optics*, Wiley, New York, 1986.

14. G. E. Gaides, Ph.D. Dissertation, University of Illinois, Urbana (1992).

15. M. Born and E. Wolf, *Principles of Optics*, Pergamon, New York, 1989.

16. C. S. Tsay and A. J. McHugh, *I&EC Res.*, **31**, 449 (1992).

17. A. J. McHugh and A. J. Spevacek, *J. Polym. Sci. Polym. Lett. Ed.*, **25**, 105 (1987).

18. L. P. McMaster, *Adv. Chem. Ser.*, **142**, Amer. Chem. Soc., Washington, D.C. 1975, p. 43.

19. R. Hasegawa, M. Koga, E. Murakami, and O. Kurihara, *Maku*, **7**, 251 (1982).

20. J. Crank, *The Mathematics of Diffusion*, Oxford University Press, 2nd ed., New York, 1989.